Using geomechanical models to simulate induced seismicity: Application to CO_2 storage at In Salah, Algeria

James P. Verdon and Anna L. Stork, University of Bristol, U.K.; Rob C. Bissell, Carbon Fluids Ltd., Amersham, U.K.; Clare E. Bond, University of Aberdeen, U.K.

Summary

We demonstrate a workflow to simulate seismicity generated by CO_2 injection into the In Salah field, Algeria. Seismic activity in hydrocarbon reservoirs is caused by stress changes on pre-existing fractures that lead to their re-activation. As inputs to our workflow, a history-matched reservoir flow simulation is used to model changes in pressure caused by injection; while a geomechanical model gives the stress state at each node of the flow model. The locations, lengths, and orientations of pre-existing fractures in the reservoir are modeled via a mass-spring solver, which restores the faulted, folded reservoir to its initial, undeformed conditions. This algorithm predicts the intensity and orientation of strain through the model, from which fracture sets can be generated. To simulate seismicity during CO_2 injection, we compute changes in effective stress caused by pore pressure changes, and map these stress changes into shear and normal stresses acting on the fractures. Where stresses exceed Mohr-Coulomb failure criteria, seismic events are predicted. We compare our modeled events with observed seismicity at In Salah, finding excellent agreement between model and observation in terms of event timing, event location, and event magnitude.

Introduction

The injection of fluids into the subsurface is becoming increasingly common. Fluids can be injected to stimulate fractures in tight reservoirs, or to enhance production from mature conventional reservoirs. Waste fluids are also being injected for storage in deep aquifers. As such, there is a clear need to be able to model, and to monitor, the geomechanical impact of subsurface injection.

Geomechanical deformation is commonly modeled numerically with finite element simulators. Reservoir models simulate pore pressure changes, which act as loading for a geomechanical model. There are many 'tunable' parameters at play in such systems, meaning that they must be calibrated with field observations for them to be considered reliable.

A range of geodetic and geophysical observations can be used to image geomechanical deformation. Seismic (and microseismic) events represent a direct indication that deformation is occurring in the reservoir. There is therefore a clear utility in linking observations of seismic activity in the field with geomechanical models. This can be done via the prediction of seismic activity using such models.

In Salah

CO_2 was injected at In Salah from 2004 – 2011, and over 3.8 million tons have been stored via 3 injection wells. The storage operation is described in detail by Mathieson et al. (2010). Initial indications of deformation came from satellite observations of ground surface motions (Onuma & Ohkawa, 2009). Of particular concern was the suggestion, implied by inversion of surface deformation data, of an actively deforming fracture network near to injection well KB502 (Vasco et al., 2010). In 2009 a microseismic monitoring array was installed near to this well to address these concerns. Barring short intervals where the array was not operational microseismic data was recorded from August 2009 until the end of injection in KB502 in 2011 (details in Stork et al., 2013).

Workflow

It is commonly understood that seismic activity in hydrocarbon reservoirs occurs on pre-existing faults and/or fractures. Pore pressure changes in the reservoir change the effective stress both in and around the reservoir, which can change both the normal and shear stress acting on these fractures. Where stresses exceed the Mohr-Coulomb failure criteria, the fracture can slip and a seismic event occurs.

On this understanding, if the locations of pre-existing fractures in and around a reservoir are known, and the changes in effective stress caused by injection and/or production can be modeled, then it should be possible to simulate when and where fractures exceed the failure envelope and trigger a seismic event. This approach forms the basis of the workflow we have developed.

This approach requires that the location, size and orientation of fractures in the reservoir are known (or can be assumed). As input to our workflow we use the fracture sets modeled by Bond et al. (2013). A structural model of the faulted, folded reservoir is generated from seismic reflection data. A mass-spring solver is used to restore the model to an unfaulted template. The restored surface is then forward modeled using the same algorithm to predict the distribution of strain orientation and intensity through the model. Fracture sets are then generated from this strain data. Bond et al. (2013) simulate the position, length and orientation of over 310,000 fractures in the In Salah reservoir.

We use a history-matched reservoir model to simulate changes in pore pressure during injection (Bissell et al.

DOI http://dx.doi.org/10.1190/segam2014-0078.1

2011). This model also generates the initial applied stress at each model node prior to injection. The reservoir model outputs a map of pore pressure on a monthly basis. We compute the effective stress (σ'_{ij}) at each node of the model from the initial applied stress (σ_{ij}) and the updated pore pressure ($P(t)$):

$$\sigma'_{ij} = \sigma_{ij} - IP(t),$$

where I is an identity matrix.

Each fracture takes its stress conditions from the nearest node in the fluid flow model. Langenbruch et al. (2013) show how natural material heterogeneity leads to variability in both principal stress magnitude and orientation where uniform external stresses are applied. Therefore, the stresses from the reservoir model are modulated for each individual fracture. This modulation takes the form of a modification in the magnitude of each principal stress by a value randomly selected between ±10%, and Euler rotations of the principal stress coordinate system by a values randomly selected between ±10°.

Having modeled σ'_{ij} at each fracture, we compute the shear (τ) and normal stress (σ_n):

$$-t = \sigma'_{ij}\, n,$$
$$-\sigma'_n = (t.n)n,$$
$$-\tau = t - \sigma'_n,$$

where n is a unit vector normal to the fracture face. The Mohr Coulomb properties, cohesion (C) and friction coefficient (μ) are defined for each fracture, selected from a normal distributions with a mean of 0.6 and standard deviation of 0.1 for μ, and a mean of 2.2MPa and standard deviation of 0.5MPa for C.

If the Mohr-Coulomb criteria are exceeded for a fracture, a seismic event is deemed to have occurred at that point. Where an event is declared, the slip direction (and thereby the rake) is determined from the orientation of the shear stress vector on the fracture plane. The strike and dip are provided by the fracture orientation, meaning that a double couple source mechanism is fully defined.

The stress drop ($\Delta\sigma$) for an event is determined as a percentage of the total shear stress acting on the fracture. This percentage is selected randomly from a uniform distribution of between 0 – 100%. The size of the rupture is also selected from a uniform distribution of between 0 – 100% of the fracture area. The seismic moment released can then be determined from:

$$M_O = (1/C)\, \Delta\sigma A^{3/2},$$

where A is the rupture area and C is a geometric constant of order unity (Kanamori & Brodsky, 2004).

A seismic event on a fracture will serve to release stress, reducing the likelihood of further seismicity on this plane. This is accounted for in our modeling approach. For fractures on which an event has occurred, the stress state at subsequent time-steps is modulated by subtracting the shear stress dropped in the previous event from the effective stress tensor. This means that a single point may slip once, and then slip again later in the simulation if pore pressure continues to increase (e.g. Goertz-Allmann et al., 2013).

Results

We focus on events triggered around injection well KB502 (which is where microseismic monitoring is focused in the field), from August 2009 to January 2011, which is the period the monitoring array was active. Figure 1 shows a map view of modeled event locations (UTM coordinate system), colored by occurrence time.

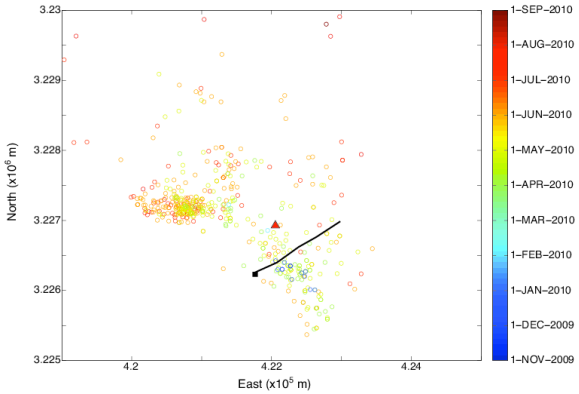

Figure 1: Map view of modeled event locations, colored by occurrence time. Horizontal injector KB502 is marked by the black line, while the microseismic monitoring well is marked by the red triangle.

We will compare our modeled events with observations from In Salah (described by Stork et al., 2013). In Figure 2a we plot a histogram of modeled event occurrence time, and compare this to observed occurrence time in Figure 2b. We note that our model does a good job in matching the relative rate of occurrence of seismicity during the monitoring period.

Sadly, limitations and technical issues with the monitoring array mean that event locations could not be resolved accurately at In Salah. As a proxy for location, Stork et al. (2013) consider the azimuths and inclinations of arriving P-waves, and the time differential between P and S wave arrivals. These are shown for observed events in Figure 3b. In order to make comparisons to our modeled event locations, we use a finite difference waveform simulator, E3D (Larsen & Harris, 1993). Taking our modeled event locations as sources, we simulate the resulting waveforms arriving at the single geophone through an isotropic, 1D

DOI http://dx.doi.org/10.1190/segam2014-0078.1

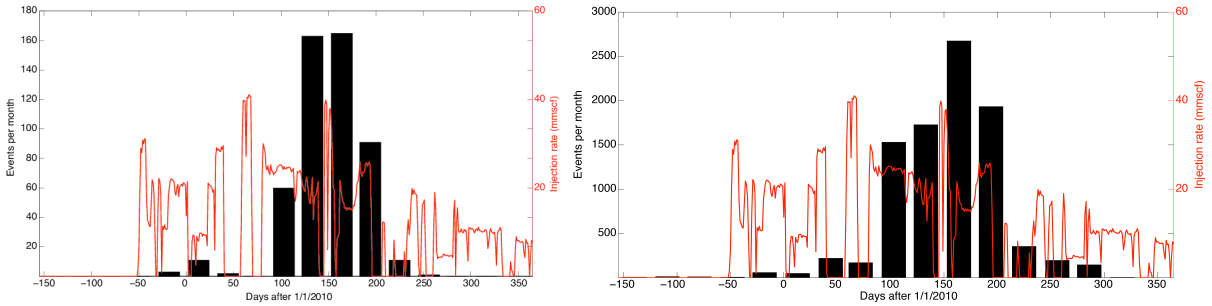

Figure 2: Modeled (a) and observed (b) event occurrence rates by month (bars). Daily injection rates in KB502 are also plotted (red). We note an excellent comparison between observed and modeled relative rates of seismicity during the monitoring period.

layered velocity model. The modeled differential S – P time and the arrival inclinations are computed from these waveforms, allowing us to make a direct comparison with Stork et al. (2013)'s observations.

In Figure 3a we show arrival angles and S – P time differentials for our modeled events. We note broad agreement in the major features between modeled (3a) and observed (3b) datasets. S – P travel times are ~0.65s for events with inclination ~0° (implying they are sited directly underneath the monitoring geophone), extending to ~1.0s for events arriving from more oblique angles. For both cases the mean azimuth (shown by dashed red lines) is ~110°. The good match between modeled and observed characteristics indicates that our modeled events are occurring in similar locations to the observed events.

In Figure 4 we plot the double couple source mechanisms for our modeled events. Events are dominantly either left lateral (rake ≈ 0°) or right lateral (rake ≈ 180°) strike slip, and occur on near-vertical planes striking between 90° - 180°. Source mechanisms have not been computed for observed events at In Salah, so we are not able to compare our modeled mechanisms with observation.

In Figure 5 we plot the frequency-magnitude relationship for our modeled events. The largest simulated event has a magnitude of M_W = 1.75. This compares favorably with observed magnitudes at In Salah, where the largest event was M_W = 1.68 (Stork et al., 2013). We fit our modeled event population with a Gutenberg-Richter relationship using the Kolmogorov-Smirnov method described by Verdon (2013), finding a b-value of 2.1. This compares well with observation at In Salah, where a b-value of 2.0 was observed. However we note that our frequency magnitude distribution might be better fitted with other,

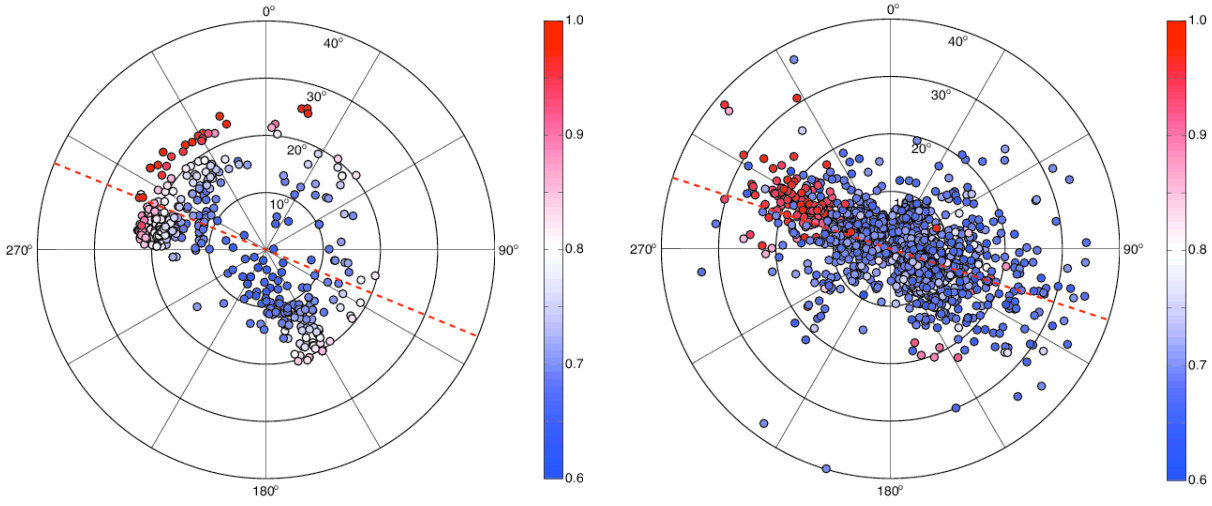

Figure 3. Modeled (a) and observed (b) event azimuths (polar angle) and inclinations (radial position). Events are colored by differential S – P arrival time. Dashed red lines highlight mean arrival azimuths

DOI http://dx.doi.org/10.1190/segam2014-0078.1

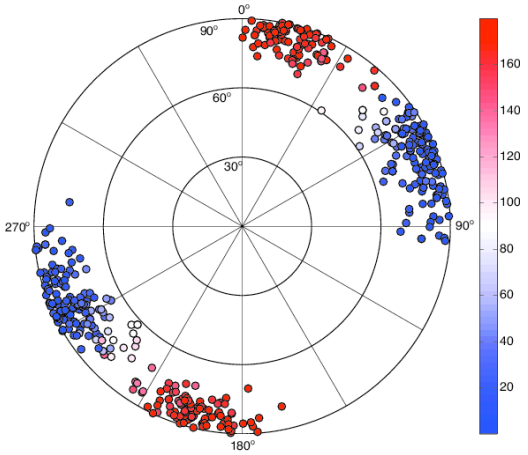

Figure 4: Modeled source mechanisms. Points represent the azimuth and dip of poles to the fracture planes, colored by their rake angles. The dominant mechanism is strike-slip, occurring on near-vertical planes striking at 90-180°.

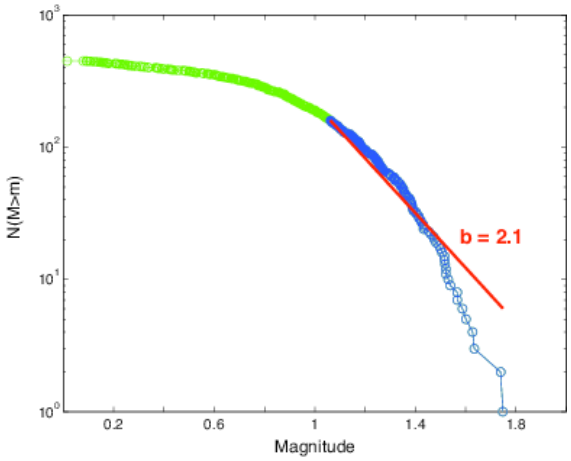

Figure 5: Frequency-magnitude relationship for our modeled event population. The largest event has a magnitude of 1.75, and can be fit with a Gutenberg-Richter b-value of 2.1.

non-fractal statistical distributions. Future work will include investigating the choice of rupture area and stress-drop distributions, such that a better match with the power-law behavior, as observed in most earthquake populations, is generated.

Nevertheless, we note that significant effort has been expended in recent years in attempting to predict the maximum magnitude earthquake that could be induced by injection activities (e.g., McGarr, 2014; Hallo et al., 2014). We note that, for this case study, our approach produces a close match between modeled and observed maximum magnitude.

Conclusions

We have demonstrated a workflow capable of simulating seismic activity in deforming reservoirs. This method resolves stresses computed by finite element geomechanical models onto simulated fracture networks, predicting seismicity when stresses exceed the Mohr-Coulomb criteria on these fractures. We have demonstrated this method by applying it to observations of seismicity during CO_2 injection at In Salah. We find that our model reproduces the key aspects of observed seismicity, including when events occur, where they occur, and the magnitudes of events.

Acknowledgements

The authors would like to thank BP for providing the microseismic observations from In Salah, as well as the reservoir simulation. JV is a Natural Environment Research Council Early-Career Research Fellow (Grant NE/I021497/1) and ALS is funded by a NERC Partnership Grant (Grant NE/I010904). This work was conducted under the aegis of the Bristol CO_2 Group (BCOG).

DOI http://dx.doi.org/10.1190/segam2014-0078.1

http://dx.doi.org/10.1190/segam2014-0078.1

EDITED REFERENCES

Note: This reference list is a copy-edited version of the reference list submitted by the author. Reference lists for the 2014 SEG Technical Program Expanded Abstracts have been copy edited so that references provided with the online metadata for each paper will achieve a high degree of linking to cited sources that appear on the Web.

REFERENCES

Bissell, R. C., D. W. Vasco, M. Atbi, M. Hamdani, M. Okwelegbe, and M. H. Goldwater, 2011, A full field simulation of the In Salah gas production and CO_2 storage project using a coupled geomechanical and thermal fluid flow simulator: Energy Procedia, **4**, 3290–3297, http://dx.doi.org/10.1016/j.egypro.2011.02.249.

Bond, C. E., R. Wightman, and P. S. Ringrose, 2013, The influence of fracture anisotropy on CO_2 flow: Geophysical Research Letters, **40**, no. 7, 1284–1289, http://dx.doi.org/10.1002/grl.50313.

Goertz-Allmann, B. P., and S. Wiemer, 2013, Geomechanical modeling of induced seismicity source parameters and implications for seismic hazard assessment: Geophysics, **78**, no. 1, KS25–KS39, http://dx.doi.org/10.1190/geo2012-0102.1.

Hallo, M., I. Oprsal, L. Eisner, and M. Y. Ali, 2014, Prediction of magnitude of the largest potentially induced seismic event: Journal of Seismology, http://dx.doi.org/10.1007/s10950-014-9417-4.

Kanamori, H., and E. E. Brodsky, 2004, The physics of earthquakes: Reports on Progress in Physics, **67**, no. 8, 1429–1496, http://dx.doi.org/10.1088/0034-4885/67/8/R03.

Langenbruch, C., and S. A. Shapiro, 2013, Relation between elastic heterogeneity, stress, and the Gutenberg-Richter b-value: A b-value estimation using sonic logs: 4th Passive Seismic Workshop, EAGE, Extended Abstracts, PS26.

Larsen, S., and D. Harris, 1993, Seismic wave propagation through a low-velocity nuclear rubble zone: Lawrence Livermore National Laboratory.

Mathieson, A., J. Midgley, K. Dodds, I. Wright, P. Ringrose, and N. Saoul, 2010, CO_2 sequestration monitoring and verification technologies applied at Krechba, Algeria: The Leading Edge, **29**, 216–222, http://dx.doi.org/10.1190/1.3304827.

McGarr, A., 2014, Maximum magnitude earthquakes induced by fluid injection: Journal of Geophysical Research, **119**, 1008–1019.

Onuma, T., and S. Ohkawa, 2009, Detection of surface deformation related with CO_2 injection by DInSAR at In Salah, Algeria: Energy Procedia, **1**, no. 1, 2177–2184, http://dx.doi.org/10.1016/j.egypro.2009.01.283.

Stork, A. L., J. P. Verdon, and J.-M. Kendall, 2013, Study of recorded seismicity at the In Salah (Algeria) carbon capture and storage project: 2nd Sustainable Earth Science Conference, EAGE, Extended Abstracts, A021.

Vasco, D. W., A. Rucci, A. Ferretti, F. Novali, R. C. Bissell, P. S. Ringrose, A. S. Mathieson, and I. W. Wright, 2010, Satellite-based measurements of surface deformation reveal fluid flow associated with the geological storage of carbon dioxide: Geophysical Research Letters, **37**, no. 3, L03303, http://dx.doi.org/10.1029/2009GL041544.

Verdon, J. P., 2013, Fractal dimension of microseismic events via the two-point correlation dimension, and its correlation with b-values: 4th Passive Seismic Workshop, EAGE, Extended Abstracts, PS25.